Stability Analysis of Unbalanced Distribution Systems With Synchronous Machine and DFIG Based Distributed Generators

Ehsan Nasr-Azadani, *Student Member, IEEE,* Claudio Cañizares, *Fellow, IEEE,*
Daniel Olivares, *Student Member, IEEE,* and Kankar Bhattacharya, *Senior Member, IEEE*

***Abstract*—There are many technical aspects and challenges in distributed generation (DG) that have not been properly understood and addressed so far. Distribution systems cannot be considered as balanced three-phase systems, because these are inherently unbalanced in steady-state operation. A full characterization of the unbalanced system with respect to system stability allows a better understanding of the dynamic behaviour of such systems. This paper presents a comprehensive investigation of the effects of system unbalance on the stability of the distribution systems with synchronous generator (SG) and doubly-fed induction generator (DFIG) based DG units at different loading levels. Detailed steady-state and dynamic analyses of the system are performed. Based on classical voltage, small-perturbation and transient stability studies, it is demonstrated that system unbalance can significantly affect the distribution system dynamic performance, in ways that have not been discussed in the technical literature so far. A simple and effective control strategy based on an Unbalanced Voltage Stabilizer (UVS) is also proposed to improve the system control and the stability of unbalanced distribution systems with SG and DFIG. Eigenvalue analyses and time-domain simulations demonstrate the effectiveness of the proposed UVS for unbalance conditions.**

***Index Terms*—Stability studies, unbalanced power systems, distributed generation, doubly-fed induction generator, voltage control.**

I. Introduction

SINCE the beginning of the 1990s, there has been significant growth of distributed generation (DG), driven by environmental and economic factors resulting in significant penetration of small scale generation at the distribution system level. Penetration of DGs in distribution systems make them active systems, instead of passive. This can affect the dynamics of the whole power system, and especially of the distribution system. Although DGs may have some benefits for the system such as improvements in system reliability, there are many technical aspects and challenges that are still not properly understood or addressed. Among the numerous issues associated with distribution systems containing DGs, stability analysis is of significant interest (e.g., [1]–[3]).

This work was supported by the NSERC Smart Microgrids Strategic Network (NSMG-Net) (www.smart-microgrid.ca) and an NSERC Discovery grant.

E. Nazr-Azadani, C. Cañizares, and K. Bhattacharya are with the Department of Electrical and Computer Engineering, University of Waterloo, Waterloo, ON, Canada, N2L 3G1 (email: enasraza@uwaterloo.ca, ccanizares@uwaterloo.ca, kankar@ece.uwaterloo.ca).

D. Olivares is with the Department of Electrical Engineering, Pontifical Catholic University, Santiago, Chile (email: dolivaresq@ing.puc.cl).

Although some stability studies of distribution systems with DGs have been reported in the literature, a detailed and systematic analysis considering distribution systems under unbalanced conditions has not been sufficiently addressed. A majority of stability studies reported in the literature are based on approaches similar to those used in transmission systems, and thus several simplifications, in particular the assumption of balanced conditions, are applied. However, distribution systems cannot be considered to be balanced three-phase systems, since these are inherently unbalanced in steady-state. A full characterization of the unbalanced system in stability analyses would allow a better understanding of its dynamic behaviour.

Nowadays, in several countries, many DGs are small synchronous generators (SGs) connected to low voltage distribution systems [4], [5]. For example, there is a significant potential for cogeneration based on small SGs from sugarcane facilities in Brazil [4]. Across Canada, many remote communities operate microgrids supplied mostly from diesel-fired SGs [6]. On the other hand, wind energy is one of the most promising renewable energy sources, with the demand for connecting wind generators to distribution systems being on the rise. Among different types of wind turbine technologies, doubly fed induction generators (DFIGs) have the largest world market share of wind turbine generators [7], offering several advantages compared to fixed-speed generators, including its ability to provide variable speed operation in a cost-effective way and independent active and reactive power control capabilities. Since the application of these DGs in distribution systems may result in different issues such as electromechanical oscillations, understanding the dynamic behaviour of SGs and DFIGs under unbalanced conditions in a distribution system is of interest to many utilities and grid operators.

A few reported studies consider the characteristics of distribution systems in stability analyses taking into account unbalanced loads and lines. In [8], a continuation three-phase power flow approach in polar coordinates is presented for voltage stability analysis under unbalanced conditions; this approach is based on static power flow equations of a three-phase model to obtain PV curves. In [9], voltage stability studies are presented using a three-phase constrained optimal power flow which seeks to maximize the loading factor. Since these studies are based on static power flows, the impact of system dynamics on voltage stability is not fully investigated.

There are recent studies of the effect of unbalanced conditions on small-perturbation stability of SGs. Thus, in [10] and [11], the effect of unbalanced conditions on damping factors and frequency is investigated. In [10], a model-based approach in the phasor domain for small-perturbation stability analysis of unbalanced distribution systems is presented, and a model identification technique for small-perturbation stability studies are presented in [11]. However, in these papers, the effects of unbalanced conditions under high loading levels, which would typically lead to instability, are not studied.

Simplified models of synchronous and induction machines have been developed for transient stability studies of unbalanced power systems [12]–[15]. These models represent the fundamental frequency component of the machine behavior and neglect the harmonic components. Based on these models, some authors analyze the impacts of DGs on transient stability. Thus, in [16] and [17], the impact of induction generators on transient stability is studied, and [18] addresses the impact of DG on transmission systems transient stability, wherein increasing the DG penetration level is matched by a reduction in centralized power generation, which consequently results in a reduction in the total amount of rotating mass and reactive power support in the system. Most of the existing transient stability studies with DGs consider different fault types under balanced loading conditions. For example, brief studies on transient stability analysis of a distribution system with selected DG units based on the calculation of critical clearing time (CCT) are presented in [3] and [19]. However, the impact of load unbalancing on transient stability studies has not been properly studied.

Control and stability studies of DFIGs have been discussed in the last decade for balanced operation [20]–[24]. However, if voltage unbalance is not properly compensated by system controls, the stator current can be highly unbalanced even with a small unbalanced stator voltage. In such case, the main problem is that high current, torque, and power oscillations appear at double the electrical frequency due to the negative sequence components, resulting in disconnection [25]–[27]. Techniques have been proposed to mitigate these oscillations, based on the injection of negative sequence components, considering rotor-side [26] or grid-side converters [25], [27]. In [28], an approach based on a disturbance rejection controller is presented to compensate oscillations using a feed-forward component of the current controllers. In [29], a stand-alone DFIG under unbalanced conditions is studied, with the grid converter supplying reactive power to compensate for the unbalanced grid voltage. A small signal stability analysis of a DFIG wind turbine is presented in [30]. In all these papers, the effects of unbalanced conditions under high loading levels, which would typically lead to instability, are not studied.

Based on the aforementioned shortcomings identified in the existing technical literature, comprehensive studies considering the dynamic behaviour of SG and DFIG based DGs under unbalanced conditions in distribution systems are presented here. This is an issue for some utilities (e.g., Hydro One Remote Communities, in Ontario, Canada), who have special interest on the stability analyses of unbalanced distribution systems with SG and DFIG DGs, since some of their feeders present unbalances as high as 25% per phase under certain conditions. Therefore, this paper presents, for the first time, comprehensive studies on voltage, small-perturbation, and transient stability of unbalanced distribution systems with SG and DFIG based DGs. Both dynamic and static voltage stability analyses are carried out using three-phase PV curves and maximum system loadability, and transient stability studies are performed using time domain simulations of contingencies under various unbalanced conditions, based on three-phase detailed models. Small-perturbation stability studies are carried out using a model identification approach to compute eigenvalues and thus study the impact of load unbalancing in heavily loaded systems. Finally, control strategies based on simple and easy to implement Unbalanced Voltage Stabilizers (UVSs) are proposed to improve the stability of unbalanced distribution systems with DGs, using time-domain simulations to demonstrate their effectiveness. Hence, the main contributions of the paper can be summarized as follows:

- A new application of three-phase power flow and dynamic voltage stability using time domain simulations is presented. A static three-phase power flow with proper DG models for voltage stability studies is used to determine maximum system loadbility under various unbalanced conditions.
- The application of an identification approach, based on Prony and Steiglitz-McBride iteration methods, for small-perturbation stability studies of unbalanced systems with DGs is proposed. This method provides a framework for small-perturbation stability analysis of unbalanced systems with DGs.
- A comprehensive evaluation of voltage stability, eigenvalue analyses, and time domain simulations for a typical distribution system with SG and DFIG based-DGs is presented under various unbalanced conditions.
- Existing control techniques to compensate the negative impact of unbalanced operation of DFIGs are demonstrated to be ineffective at heavily loaded conditions. Furthermore, simple and effective control strategies based on voltage unbalance for both SG and DFIG based-DGs are proposed to improve the stability of the distribution systems. The simplicity of the proposed UVS makes it practical and relatively easy to implement in real systems.

The rest of paper is organized as follows: A brief overview of the system model and the methodology used for stability analyses under unbalanced conditions are presented in Section II; the proposed unbalanced voltage stabilizer control is also discussed in this section. In Section III, comprehensive numerical results with different scenarios for a DG-load-grid system are presented and discussed. Finally, Section IV highlights the main contributions and conclusions of the paper.

II. System Modeling, Analysis and Control Methodology

A. SG and Network Models

Detailed representation of the SG model is used for the simulations and studies [31]; hence, three-phase stator and rotor windings in the *dqo* reference-frame are used [32]. Since small

SG based DGs are very likely to have simple Proportional-Integral (PI) voltage regulators, Automatic Voltage Regulators (AVRs) Type IV (AC4A) are used here. Moreover, the type of voltage feedback in the excitation system affects the dynamic behavior of the system [33], a typical voltage feedback represented by the average value of the voltage magnitude for each phase is used in this paper [31].

Lines are modeled as constant coupled impedance branches, and loads are treated as constant impedances as well. Therefore, the following loading factor l is defined to model load impedance Z_l increases in each phase, which increase the active and reactive power demand:

$$Z_l = \frac{Z_\phi}{l} \tag{1}$$

where Z_ϕ is the base-load impedance for each phase. A load unbalance factor is defined to analyze different scenarios of unbalance as the load varies [10]. Thus, as the impedance of the load in one phase is increased, the load impedance in another phase is decreased, so that total impedance of the three-phase load remains constant in all cases, as follows:

$$Z_{al} = (1+k)Z_l \tag{2}$$

$$Z_{bl} = Z_l \tag{3}$$

$$Z_{cl} = (1-k)Z_l \tag{4}$$

where k is the load unbalance factor, and Z_{al}, Z_{bl}, and Z_{cl} are the phase impedances of the load.

B. DFIG Model

The DFIG is modeled using a classical and detailed induction machine model with a wound rotor [32], and a detailed model of the back-to-back ac/ac converter controlling the rotor [34]. Unbalance loading in DFIGs introduce negative sequence components in the voltage, current, and flux, which can result in significant oscillations in torque, active and reactive power with a double frequency; hence, a DFIG model that considers the positive and negative sequence components is needed to study this phenomenon. This is accomplished using a three-phase signal in the stationary $\alpha\beta$ reference-frame expressed by the positive and negative sequence components as follows:

$$\begin{aligned}\begin{bmatrix} F_\alpha(t) \\ F_\beta(t) \end{bmatrix} &= \begin{bmatrix} F_\alpha^+(t) + F_\alpha^-(t) \\ F_\beta^+(t) + F_\beta^-(t) \end{bmatrix} \\ &= F_{\alpha\beta}^+ e^{j(\omega_e t)} + F_{\alpha\beta}^- e^{-j(\omega_e t)}\end{aligned} \tag{5}$$

where F represents voltage, current, or flux linkage; t is time; and ω_e is electrical angular frequency. There are two approaches for the positive and negative sequence components separation under unbalanced conditions: separation by low pass filter (LPF), and separation by a signal delay cancellation [27]. In this paper, the positive and negative sequence components separation is based on a LPF approach, in which, as the negative sequence components appear with the frequency $2\omega_e$ in the positive dq reference-frame, and the positive sequence appears with the frequency $2\omega_e$ in the negative dq reference-frame, a LPF can be used to bypass dc components for both sequences. Thus, the stator components (i.e., current, voltage, and flux) in the positive and negative sequence $\alpha\beta$ reference-frame yield:

$$\begin{aligned} F_{\alpha\beta}^+ &= F_{dq}^+ + F_{dq}^- e^{-j2\omega_e t} \\ F_{\alpha\beta}^- &= F_{dq}^- + F_{dq}^+ e^{-j2\omega_e t}\end{aligned} \tag{6}$$

The d-axis for the positive sequence in the dq reference-frame is fixed to the positive sequence of stator flux rotating at the speed ω_e, while the d-axis for the negative sequence rotates at $-\omega_e$. Based on two rotating reference-frames at ω_e and $-\omega_e$, the voltage equations for the positive and negative sequences at the grid side can be written as:

$$\begin{aligned} v_{gdq}^+ - v_{cdq}^+ &= (R_g + j\omega_e L_g) i_{gdq}^+ + L_g \frac{di_{gdq}^+}{dt} \\ v_{gdq}^- - v_{cdq}^- &= (R_g + j\omega_e L_g) i_{gdq}^- + L_g \frac{di_{gdq}^-}{dt}\end{aligned} \tag{7}$$

where v is voltage; i is current; g is the grid side; c is the converter side; R_g is grid resistance; and L_g is grid inductance. Also, the voltage equations for the positive and negative sequences at the rotor and the stator sides are:

$$\begin{aligned}\begin{bmatrix} v_s^+ \\ v_r^+ \end{bmatrix} &= \begin{bmatrix} L_s & L_m \\ L_m & L_r \end{bmatrix} \frac{d}{dt} \begin{bmatrix} i_s^+ \\ i_r^+ \end{bmatrix} \\ &+ \begin{bmatrix} R_s + jL_s\omega_e & jL_m\omega_e \\ jL_m(\omega_e - \omega_r) & R_r + jL_r(\omega_e - \omega_r) \end{bmatrix} \begin{bmatrix} i_s^+ \\ i_r^+ \end{bmatrix}\end{aligned} \tag{8}$$

$$\begin{aligned}\begin{bmatrix} v_s^- \\ v_r^- \end{bmatrix} &= \begin{bmatrix} L_s & L_m \\ L_m & L_r \end{bmatrix} \frac{d}{dt} \begin{bmatrix} i_s^- \\ i_r^- \end{bmatrix} \\ &+ \begin{bmatrix} R_s - jL_s\omega_e & -jL_m\omega_e \\ jL_m(-\omega_e - \omega_r) & R_r + jL_r(-\omega_e - \omega_r) \end{bmatrix} \begin{bmatrix} i_s^- \\ i_r^- \end{bmatrix}\end{aligned} \tag{9}$$

where s stands for the stator; r stands for the rotor; L_s is stator inductance; L_r is rotor inductance; and L_m is mutual inductance. Based on (8) and (9), the stator output active and reactive power under unbalance conditions can be written as:

$$P_s = \frac{3}{2}\left[P_{s_0} + P_{ssin}\sin 2(\omega_e t) + P_{scos}\cos 2(\omega_e t)\right] \tag{10}$$

$$Q_s = \frac{3}{2}\left[Q_{s_0} + Q_{ssin}\sin 2(\omega_e t) + Q_{scos}\cos 2(\omega_e t)\right] \tag{11}$$

where P_s is the stator active power; Q_s is the stator reactive power; and:

$$\begin{bmatrix} P_{s_0} \\ Q_{s_0} \\ P_{ssin} \\ P_{scos} \\ Q_{ssin} \\ Q_{scos} \end{bmatrix} = \begin{bmatrix} v_{sd}^+ & v_{sq}^+ & v_{sd}^- & v_{sq}^- \\ v_{sq}^+ & -v_{sd}^+ & v_{sq}^- & -v_{sd}^- \\ v_{sq}^- & -v_{sd}^- & -v_{sq}^+ & v_{sd}^+ \\ v_{sd}^- & v_{sq}^- & v_{sd}^+ & v_{sq}^+ \\ -v_{sd}^- & -v_{sq}^- & v_{sd}^+ & v_{sq}^+ \\ v_{sq}^- & -v_{sd}^- & v_{sq}^+ & -v_{sd}^+ \end{bmatrix} \begin{bmatrix} i_{sd}^+ \\ i_{sq}^+ \\ i_{sd}^- \\ i_{sq}^- \end{bmatrix} \tag{12}$$

Since the electrical power is the sum of the power from the equivalent voltage source $j\omega_e\psi_s$ and $j(\omega_e - \omega_r)\psi_r$ [26], where ψ stands for flux linkage, the electrical torque of the DFIG can be written as:

$$T_e = P_e/\omega_r = \frac{3}{2}\frac{L_m}{L_s}\left[T_{e_0} + T_{esin}\sin 2(\omega_e t) + T_{ecos}\cos 2(\omega_e t)\right] \tag{13}$$

where T_e is the electrical torque; P_e is the electrical power; and:

$$\begin{bmatrix} T_{e_0} \\ T_{esin} \\ T_{ecos} \end{bmatrix} = \begin{bmatrix} -\psi_{sq}^{+} & \psi_{sd}^{+} & -\psi_{sq}^{-} & \psi_{sd}^{-} \\ -\psi_{sq}^{-} & \psi_{sd}^{-} & -\psi_{sq}^{+} & \psi_{sd}^{+} \\ \psi_{sd}^{-} & \psi_{sq}^{-} & -\psi_{sd}^{+} & -\psi_{sq}^{+} \end{bmatrix} \begin{bmatrix} i_{rd}^{+} \\ i_{rq}^{+} \\ i_{rd}^{-} \\ i_{rq}^{-} \end{bmatrix} \tag{14}$$

Note that, since the negative sequence of stator and rotor components are zero under balanced conditions, the sin and cos oscillating terms for the stator active and reactive power, and the electrical toque disappear.

The DFIG rotor control is based on the stator flux-oriented synchronous frame in the dq-axes. Thus, the stator flux linkage can be calculated as follows:

$$\frac{d\psi_s}{dt} = v_s - R_s i_s. \tag{15}$$

The stator flux in the polar form after Clarke's transformation can be written as:

$$|\psi_s| = \sqrt{\psi_{s\alpha}^2 + \psi_{s\beta}^2} \tag{16}$$
$$\theta_s = \tan^{-1}\left(\frac{\psi_{s\beta}}{\psi_{s\alpha}}\right)$$

where the angle θ_s is the instantaneous location of the stator flux. Note that the transformation of dq reference-frame to $\alpha\beta$ reference-frame in the rotor-side is based on $\omega_{slip} = \omega_e - \omega_r$.

The stator active and reactive powers can be independently controlled by i_{rd} and i_{rq}, respectively; thus, two PI controllers are used to control the active and reactive power. From the point of view of the reactive power, the DFIG may be in constant power factor (PF) mode, or voltage control mode. As the DFIG can control the reactive power or the output voltage, a PI controller is used to control the output voltage by controlling i_{rd}. The reference current i_{rd} and i_{rq} are converted to the $\alpha\beta$ and then to the abc reference-frames based on ω_{slip}. On the grid-side, two PI feedback controllers are used to decouple current control. Figure 1 illustrates the DFIG control scheme, where E_c is the converter dc bus voltage.

Under unbalanced conditions, there are four degrees of freedom for rotor current components, i.e., the positive and negative sequence of the rotor current components; thus, different control objectives can be chosen. It is worth noticing that it is not possible to eliminate all oscillations in the electrical torque, the active and reactive powers, and the stator current at the same time. In this paper, the main objective is to keep the electrical torque oscillations at a minimum for given active power and voltage values. Since i_{rd}^{+*} and i_{rq}^{+*} are obtained to control voltage magnitude and active power, respectively, as shown in Fig.1, and substituting $T_{esin}^{*} = T_{ecos}^{*} = 0$ in (14), the negative sequence rotor current references are given by:

$$\begin{bmatrix} i_{rd}^{-*} \\ i_{rq}^{-*} \end{bmatrix} = \begin{bmatrix} -\psi_{sq}^{+} & \psi_{sd}^{+} \\ -\psi_{sd}^{+} & -\psi_{sq}^{+} \end{bmatrix}^{-1} \begin{bmatrix} \psi_{sq}^{-} i_{rd}^{+*} - \psi_{sd}^{-} i_{rq}^{+*} \\ -\psi_{sd}^{-} i_{rd}^{+*} - \psi_{sq}^{-} i_{rq}^{+*} \end{bmatrix} \tag{17}$$

If the control target is to eliminate the stator active power oscillations, according to (12), the stator current references are:

$$\begin{bmatrix} i_{sd}^{+*} \\ i_{sq}^{+*} \\ i_{sd}^{-*} \\ i_{sq}^{-*} \end{bmatrix} = \begin{bmatrix} v_{sd}^{+} & v_{sq}^{+} & v_{sd}^{-} & v_{sq}^{-} \\ v_{sq}^{+} & -v_{sd}^{+} & v_{sq}^{-} & -v_{sd}^{-} \\ v_{sq}^{-} & -v_{sd}^{-} & -v_{sq}^{+} & v_{sd}^{+} \\ v_{sd}^{-} & v_{sq}^{-} & v_{sd}^{+} & v_{sq}^{+} \end{bmatrix}^{-1} \begin{bmatrix} P_{s_0}^{*} \\ Q_{s_0}^{*} \\ P_{ssin}^{*} \\ P_{scos}^{*} \end{bmatrix} \tag{18}$$

All time-domain simulations are carried out in PSCAD/EMTDC [31], which is a commercial time-domain software with detailed representation of generators, controllers, loads, and lines.

C. Voltage Stability Studies

It is common practice to carry out loadability studies using PV curves [35]. The continuation power flow yields these curves for voltage stability assessment by increasing the system loading level up to a maximum loadability point at which the system becomes unstable. In this paper, both dynamic and static analyses are carried out using the PV curves and maximum loadability computations. Static voltage stability studies are based on three-phase power flows; in this case, the static maximum loadability is associated with a loading level at which there is no power flow solution.

Dynamic voltage stability studies are carried out using time-domain simulations in PSCAD/EMTDC, based on the detailed dynamic models of DGs and their voltage regulators. Since the generator operates as a voltage source to compute the initial point for time-domain simulations, if the difference between the steady-state condition and the initial point is too large, it may lead to numerical instability. Thus, the initial variables of the generator (e.g., terminal voltage phase) are calculated using a static three-phase power flow, which are then used in PSCAD/EMTDC as the initial point for simulations. Since the results of time-domain simulations under steady-state conditions are needed for loadability studies, voltage and active and reactive powers should be in steady-state conditions. Hence, the results of time-domain simulations after a long settling time (20 s in this paper) are used to obtain PV curve points.

Three-phase power flow calculations are based on node voltages and branch currents. For each series element (e.g., transmission line, transformer, etc.) connecting two nodes, the node voltages and branch currents at each end can be represented by the following equation [36]:

$$\begin{bmatrix} v_a \\ v_b \\ v_c \\ i_a \\ i_b \\ i_c \end{bmatrix}_s = \begin{bmatrix} [A] & [B] \\ [C] & [D] \end{bmatrix}_l \begin{bmatrix} v_a \\ v_b \\ v_c \\ i_a \\ i_b \\ i_c \end{bmatrix}_r = [ABCD]_l \begin{bmatrix} v_a \\ v_b \\ v_c \\ i_a \\ i_b \\ i_c \end{bmatrix}_r \tag{19}$$

where $[ABCD]_l$ is the three-phase equivalent ABCD-parameter matrix of the series element; v_a, v_b, v_c are line-to-ground voltage phasors; and i_a, i_b, i_c are line current phasors. Based on the π-model of feeders depicted in Fig.2, the three-phase ABCD-parameter matrices of the feeders can be calculated as follows:

$$[A] = I_3 + \frac{1}{2}[Z_{abc}][Y_{abc}] \tag{20}$$

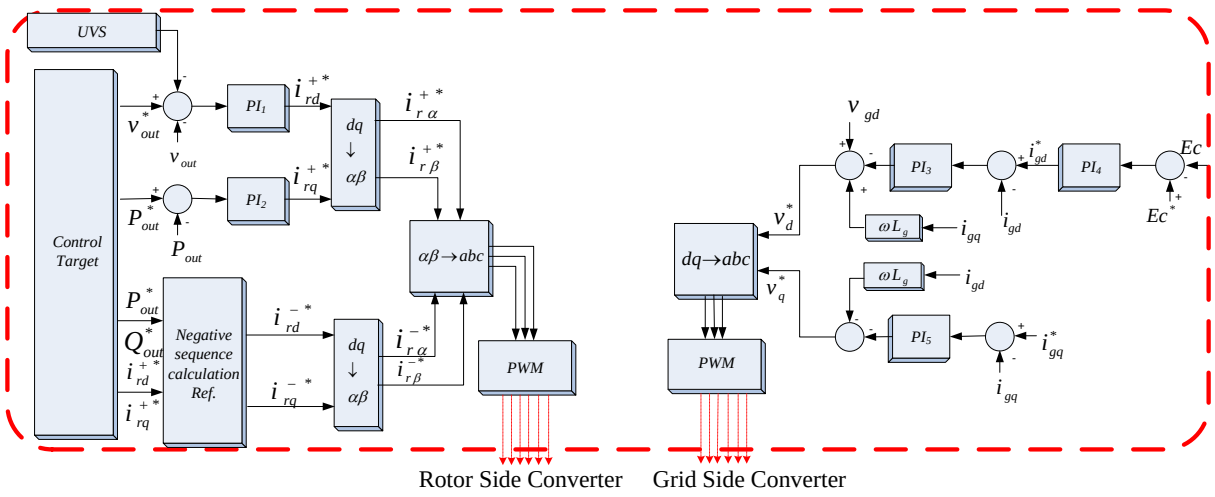

Fig. 1. Control scheme of the DFIG under unbalanced conditions.

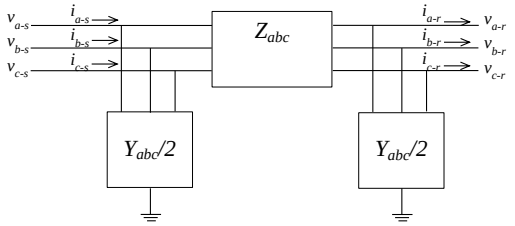

Fig. 2. Series element π-model.

$$[B] = [Z_{abc}] \tag{21}$$

$$[C] = [Y_{abc}] + \frac{1}{4}[Y_{abc}][Z_{abc}][Y_{abc}] \tag{22}$$

$$[D] = I_3 + \frac{1}{2}[Z_{abc}][Y_{abc}] \tag{23}$$

where I_3 is the 3×3 identity matrix. Matrices $[Z_{abc}]$ and $[Y_{abc}]$ in (20)-(23) can be approximated from the sequence-reference-frame diagonal impedance matrices $[Z_{seq}]$ and $[Y_{seq}]$, respectively, as follows:

$$[Z_{abc}] = [A][Z_{seq}][A]^{-1} \tag{24}$$

$$[Y_{abc}] = [A][Y_{seq}][A]^{-1} \tag{25}$$

where

$$[A] = \begin{bmatrix} 1 & 1 & 1 \\ 1 & a^2 & a \\ 1 & a & a^2 \end{bmatrix}; a = 1\angle 120 \tag{26}$$

SGs can be modeled as a special case of series elements connecting the internal bus voltages to terminal voltages through a series impedance. The series impedance of a generator in the abc reference-frame can be calculated from the sequence-reference-frame impedances as shown previously, where sequence impedances are obtained from machine parameters [37]. Internal bus voltages are assumed to be balanced, which is modeled using the following equations:

$$|e_a| = |e_b| = |e_c| \tag{27}$$

$$e_a + e_b + e_c = 0 \tag{28}$$

It is important to note that the (27) and (28) also hold for a negative-sequence voltage, and a reasonable starting point for variables e_a, e_b, and e_c ensures convergence to a positive-sequence internal voltage. For modeling PV-buses, the power injected by a particular generator is assumed fixed, as follows:

$$Re\left\{ \begin{bmatrix} v_a & v_b & v_c \end{bmatrix}_G \begin{bmatrix} i_a^* \\ i_b^* \\ i_c^* \end{bmatrix}_G \right\} = P_G \tag{29}$$

Additional relations imposed by impedance loads are:

$$\begin{bmatrix} v_a \\ v_b \\ v_c \end{bmatrix}_{Load} = [Z_{Load}] \begin{bmatrix} i_a \\ i_b \\ i_c \end{bmatrix}_{Load} \tag{30}$$

where Z_{Load} is a diagonal matrix, with the phase-to-ground load impedances in the diagonal. Finally, the power flow equations are completed by applying KCL at each node of the system.

For small systems, this set of nonlinear equations can be readily implemented in Matlab [38], and solved within reasonable computational times using the `fsolve` function with different robust numerical algorithms (e.g., Trust-region and Levenberg-Marquardt).

D. Transient Stability Studies

There are various criteria to evaluate the transient stability of a system. For example, CCT can be used as an index to evaluate the system robustness [39]. The CCT represents the point beyond which, the system is unable to recover its stability if the fault clearing time is greater than the CCT. When a fault occurs in the system, the difference between the actual clearing time (assuming the system is stable) and CCT may be used to define a transient stability margin for the system. Note that the CCT is not usually used as a stand-alone index to study transient stability of power systems, but it can be used for comparative system stability analyses as in this paper. Different contingencies need to be studied to determine the worst case scenarios in the system.

E. Small-Perturbation Stability Studies

Eigenvalue analysis of the system state matrix is one of the common tools for small-perturbation stability studies. In the context of power systems, several simplifications such as system modeling under balanced conditions are applied. Thus, the system is usually modeled with single-phase equivalents, so that small-perturbation stability analysis of a balanced power system can be normally carried out by the linearization of the power system model around an equilibrium point. Many commercial programs use phasor models for small-perturbation stability studies, and assume a specific equilibrium point under steady-state conditions. In the case of unbalanced condition, equilibrium points are non-stationary with respect to the angular velocity of the SGs, since the generator velocity is sinusoidal under steady-state conditions; hence, standard phasor-based linearization techniques are not applicable in this case [10].

There are two approaches for small-perturbation stability studies under unbalanced conditions: a model based approach, and a modal estimation approach [10], [40]. In this paper, small-perturbation stability analyses are performed using modal estimations, in particular, the Prony method and the Steiglitz-McBride iteration method [41], [42], based on time-domain simulations.

As mentioned in the previous section, PSCAD/EMTDC provides data to analyze the dynamics of the system, which is then used here in an appropriate modal estimation method, i.e., Steiglitz-McBride iteration and Prony, to estimate the system eigenvalues. In the studies presented in this paper, the generator speed from time-domain simulations is used as a signal for the modal estimation method. The conventional Prony method available in Matlab is used in this paper [38].

The Prony method is suitable for transient stability studies with high signal to noise ratio (SNR). However, when the system becomes unstable, the Prony method cannot follow the signal properly. In this case, the Steiglitz-McBride iteration method has better performance. Figure 3 presents a comparison of the measured data and the estimated signal by Prony and Steiglitz-McBride iteration methods when the system is unstable. Note that the Steiglitz-McBride iteration method fits the signal well, while the Prony method is unable to extract the true poles of the signal when the system is unstable.

Since the length of the output data of the time-domain simulation is too long (e.g., 20000 points in a 10 s simulation), it is assumed that the signal is divided in sets of 0.5 s window data, with each set of data being then used in the identification methods to estimate the signal, giving a number of poles and zeros. Based on the nature of the signal and using mean-square-errors, the number of poles was set to 8 here.

F. Proposed Unbalanced Voltage Stabilizer

When a system is more heavily loaded, it can become unstable as unbalancing increases and the critical poles cross the imaginary axes, as discussed in Section III. Since this results in oscillatory modes, a UVS is proposed to mitigate these oscillations, integrating it with the generator voltage regulator to provide an auxiliary stabilizing signal.

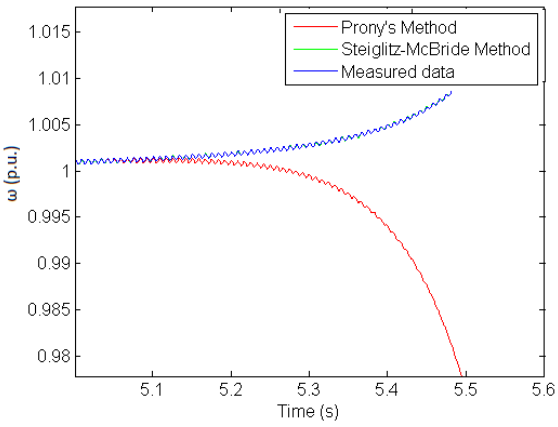

Fig. 3. Measured data and estimated signal when the system is unstable for the test system discussed in Section III.

Figure 4 shows the proposed UVS for the SG based DG. This UVS provides a damping torque component when the system is unbalanced; hence, the input signals used here are the voltage magnitudes in all phases. These are then converted to the dqo reference-frame based on:

$$\begin{bmatrix} v_d \\ v_q \\ v_o \end{bmatrix} = \begin{bmatrix} \cos(\theta) & \cos(\theta-120) & \cos(\theta-240) \\ \sin(\theta) & \sin(\theta-120) & \sin(\theta-240) \\ \frac{1}{2} & \frac{1}{2} & \frac{1}{2} \end{bmatrix} \begin{bmatrix} v_a \\ v_b \\ v_c \end{bmatrix} \quad (31)$$

For $\theta = 0$, the transformation $\sqrt{v_d^2 + v_q^2}$ can be used to reflect the degree of unbalance, since as the unbalance increases, the output signal increases as well. The gain K_{UVS} determines the damping factor provided by the UVS, and the first-order phase compensation block provides appropriate phase lead to compensate for the phase lag between the voltage regulator input and the generator electrical torque. The limits V_{UVS}^{max} and V_{UVS}^{min} constrain the output signal, which is an auxiliary negative-feedback signal for the voltage regulator, due to the fact that by decreasing the generator terminal voltages, the load demand decreases, thus reducing the system stress as demand and unbalance increase. Therefore, stability can be improved as the load increases with the proposed UVS.

The tuning of the UVS parameters would be similar to that of the power system stabilizer in power systems; thus, the gain K_{UVS} should be set to guarantee system stability, since if this gain is tuned improperly, the system may be unstable, and the time constants should be selected to compensate for the phase lags of the system. The UVS parameter values used here are provided in the Appendix.

Figure 5 shows the proposed UVS for the DFIG, based on similar principles as the SG UVS. Since the negative-sequence components of terminal voltages are available for DFIG control, these signals are used here and then converted to the dq^- reference-frame.

III. Results

A. Test System

The distribution system in the Kumamoto area in Japan from [43] shown in Fig.6, is used to develop the simplified test

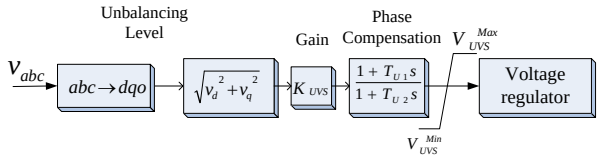

Fig. 4. Block diagram of the proposed UVS for an SG based DG unit.

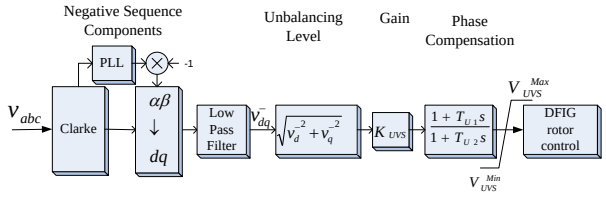

Fig. 5. Block diagram of the proposed UVS for a DFIG based DG unit.

system depicted in Fig.7. The original system has been used to test and compare various models of several types of DGs [3].

There are various distribution systems in Canada, Brazil, and Iran where there is a single SG or DFIG based DG, as is the case of the sugarcane facilities in Brazil [4] and remote feeders in Ontario. These systems can be modeled using the system depicted in the Fig.7, which contains only one generator. This system is also useful to better understand and explain stability issues associated with unbalanced DGs, one type of generator at a time. Thus, the system comprises a DG unit, feeders and load, all connected to an infinite bus representing the main grid. In order to study a contingency in the system, short-duration three-phase faults close to the load, with some impedance to ground, are simulated.

The load is modeled as constant impedance, based on rated voltage and active and reactive powers. In the base case, the active and reactive powers are $P_{Load} = 3$ MW, and $Q_{Load} = 1$ Mvar, respectively. Because of the low voltage at the load bus at high loading levels, a balanced capacitor bank is connected at the load bus; the reactive power of the bank for the base case is $Q_{cap} = 0.7$ Mvar, and increases linearly with the loading factor l. All test system parameters are given in the Appendix.

The main objective of the grid-side converter is to control

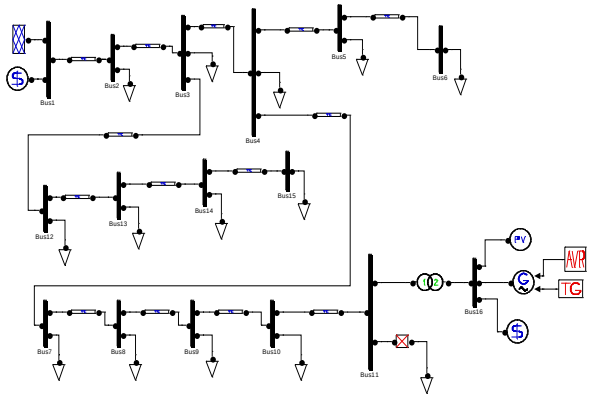

Fig. 6. Kumamoto, Japan distribution test system from [3].

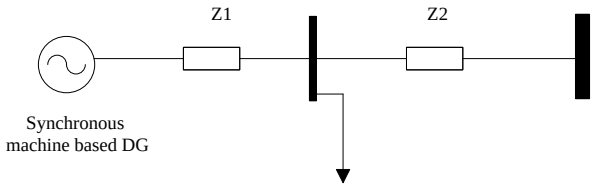

Fig. 7. Simplified test system.

the dc link voltage by controlling i_{gd}. The DFIG is assumed to be in speed control at 1.2 p.u, i.e., the rotor speed is set externally, as the large inertia of the wind turbine results in slow changes of the rotor speed. In this case, the capacitor at the load is set at $Q_{cap} = 2.17$ Mvar. To start the simulations, the rotor-side converter is first set in PF control mode and at $t = 1$ s the controller is switched to voltage control, otherwise the system is unstable.

B. Voltage Stability Analysis

The DG and slack bus (main grid) are assumed to share the injected power inversely proportional to the line impedances Z_1 and Z_2 as the load is increased, considering limits on DG active power. Table I shows the comparison of the maximum active power loadability, and loading factor for different unbalanced conditions obtained with three-phase power flow and time-domain simulations (TDS) for the SG based DGs. Table II shows the maximum loadability and the voltage magnitude in phases a, b, and c for different realistic unbalanced conditions for the SG. Observe from Table I and II that when the system unbalancing increases, the maximum loadability of the system decreases. Also, the difference between the maximum loading factors obtained from the static and dynamic studies, i.e., three-phase power flow and TDS, respectively, arise because of the effects of detailed modeling of generator and voltage regulator on TDS. The system becomes unstable due to eigenvalues crossing the imaginary axes, as discussed in detail in Section III-D, which cannot be observed in power flow studies.

Figure 8 illustrates the voltage magnitude at the load under balanced and unbalanced conditions, and Fig.9 depicts the PV curve under balanced and unbalanced condition for $k = 20\%$ for the SG. Observe that the voltage magnitude in phase b is close to the voltage magnitude for the balanced condition, and the voltage magnitudes of phases c and a are greater and less than that of phase b, respectively, as expected. The voltage magnitude in phase c is relatively high, which is due to the capacitor bank. Note that since the loads are modeled based on constant impedances, the maximum power for the system does not necessarily correspond to the maximum loading factor, due to the active and reactive powers being proportional to the square of the voltage and the loading factor. It is worth noticing that the maximum loadability of the system will be limited in practice by voltage limits, which would require additional compensation equipment. Also, the voltage differences for all phases may be compensated by per-phase capacitor banks.

Table III shows the maximum loadability and the voltage magnitudes in phases a, b, and c for different realistic un-

TABLE I
MAXIMUM ACTIVE POWERS AND LOADING FACTORS FOR DIFFERENT UNBALANCED CONDITIONS FOR STATIC THREE-PHASE POWER FLOW AND TIME-DOMAIN SIMULATIONS WITH SG.

$k(\%)$	Maximum loading factor (p.u.)		Maximum active power loadability (p.u.)	
	TDS	Three-phase PF	TDS	Three-phase PF
0	2.2	2.24	0.692	0.6925
5	2.2	2.24	0.692	0.6925
10	2.2	2.22	0.691	0.6923
15	2.2	2.22	0.691	0.6917
20	2.15	2.20	0.689	0.6912
25	2.1	2.18	0.687	0.6903

TABLE II
MAXIMUM ACTIVE POWER AND VOLTAGE MAGNITUDE IN ALL PHASES FOR DIFFERENT UNBALANCED CONDITIONS WITH SG.

$k(\%)$	Maximum active power loadability (p.u.)	V_a(p.u.)	V_b(p.u.)	V_c(p.u.)
0	0.692	1.0089	1.0089	1.0089
5	0.692	0.9836	1.0076	1.0337
10	0.691	0.9554	1.0058	1.0558
15	0.691	0.9199	0.9985	1.0709
20	0.689	0.9050	1.0172	1.1097
25	0.687	0.8826	1.0292	1.1310

balanced conditions of the distribution system with DFIG. Observe that when the system unbalancing increases, the maximum loadability of the system decreases, and the voltage magnitude differences in phases a, b, and c with respect to the voltage magnitudes in balanced conditions increase.

Figure 10 shows the voltage magnitude at the load under balanced and unbalanced conditions for $k = 15\%$ with DFIG, and Fig.11 depicts the PV curve under balanced and unbalanced condition. Observe that the voltage magnitude in phase b is close to the voltage magnitude for the balanced condition, and the voltage magnitudes of phases c and a are greater and less than that of phase b, respectively, as expected.

C. Transient Stability Analysis

Three-phase-to-ground faults of short-duration and close to the load are considered as contingencies for the SG. The simulation time is 20 s, and the fault occurs at $t = 3$ s. Table IV illustrates the CCT of the test system with the SG and the DFIG for different values of k for the base loading factor (i.e., $l = 1$ p.u.). Observe that the CCT decreases as the unbalance increases, decreasing by 30% for the SG and 95% for the DFIG as k increases from 0% to 25%. Since the power rating of the SG and the DFIG are different, the corresponding CCTs are not comparable with each other. It should be noted that, as the load increased, it was observed that the CCT remained unchanged, due to the fact that the DG is at its maximum power output at base load.

Figures 12 and 13 depict the transient behavior of the SG at

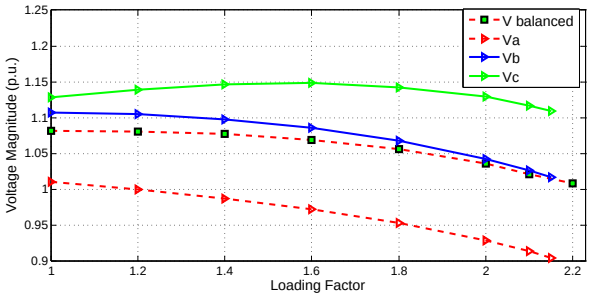

Fig. 8. Load voltage magnitude versus loading factor with SG for $k = 20\%$.

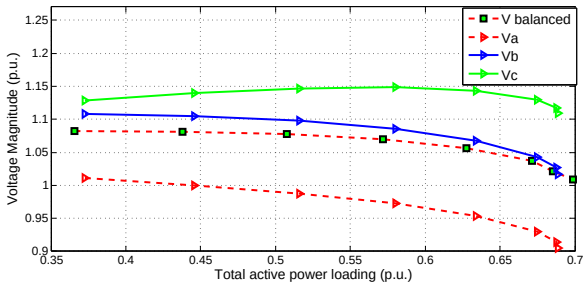

Fig. 9. PV curves with SG for $k = 20\%$.

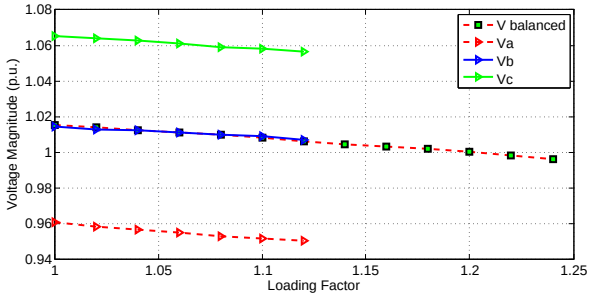

Fig. 10. Load voltage magnitude versus loading factor with DFIG for $k = 15\%$.

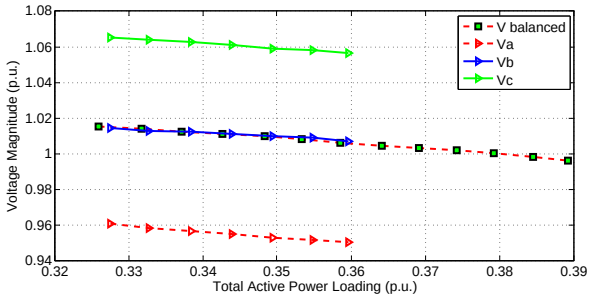

Fig. 11. PV curves with DFIG for $k = 15\%$.

TABLE III
MAXIMUM ACTIVE POWER AND VOLTAGE MAGNITUDE IN ALL PHASES FOR DIFFERENT UNBALANCED CONDITIONS WITH DFIG.

$k(\%)$	Maximum active power loadability (p.u.)	V_a(p.u.)	V_b(p.u.)	V_c(p.u.)
0	0.389	0.996	0.996	0.996
5	0.384	0.978	0.998	1.015
10	0.379	0.962	0.998	1.035
15	0.359	0.950	1.007	1.056
20	0.350	0.935	1.011	1.073
25	0.335	0.921	1.016	1.090

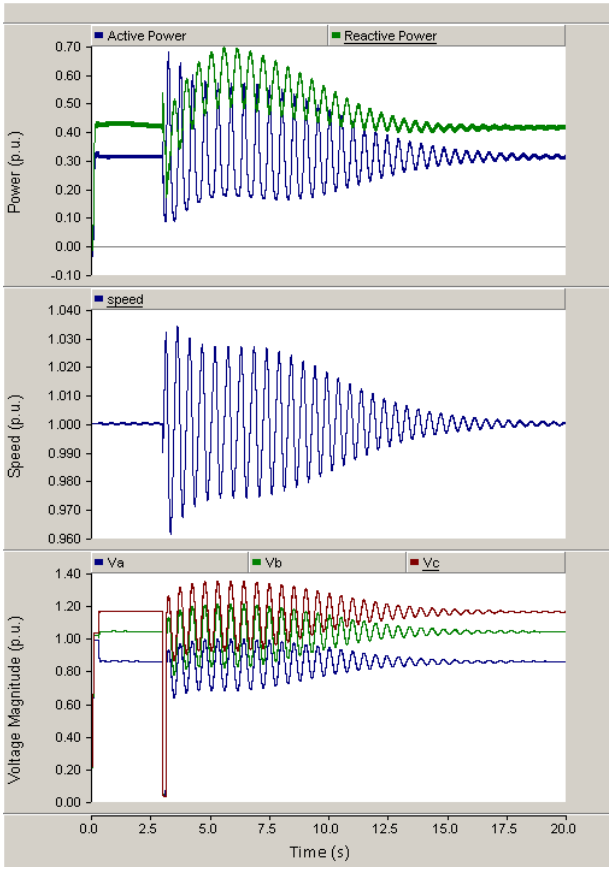

Fig. 12. Transient behavior of SG at $k = 25\%$ before CCT.

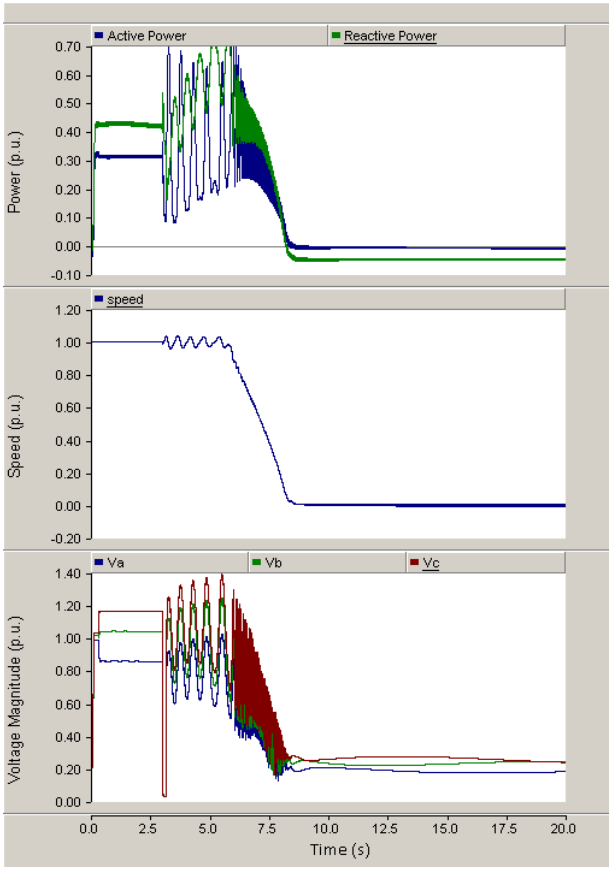

Fig. 13. Transient behavior of SG at $k = 25\%$ after CCT.

TABLE IV
CCT OF THE TEST SYSTEM AT BASE LOAD ($l = 1$ P.U.) FOR A THREE-PHASE-TO-GROUND FAULT.

$k(\%)$	CCT of the test system with the SG (s)	CCT of the test system with DFIG (s)
0	0.45	0.1
5	0.42	0.1
10	0.40	0.1
15	0.37	0.05
20	0.35	0.005
25	0.30	0.005

TABLE V
DAMPING FACTORS AND FREQUENCY OF OSCILLATIONS FOR DIFFERENT UNBALANCED CONDITIONS.

	Pole	Damping factor (%)	Frequency (rad/s)
k= 0%	-1.09 + j12.7	8.53	12.7
k=5%	-1.11 + j12.6	8.82	12.6
k=10%	-1.12 + j12.5	8.89	12.6
k=15%	-1.13 + j12.4	9.03	12.5
k=20%	-1.14 + j12.3	9.25	12.3
k=25%	-1.16 + j12.0	9.65	12.1

a loading factor $l = 1.5$ p.u. and $k = 25\%$ for the studied fault before and after the CCT. Observe that the system is stable for a clearing time 0.12 s, and unstable for clearing times greater than 0.12 s.

D. UVS Impact on SG

Two scenarios are considered to analyze the effects of unbalanced conditions on small-perturbation stability for the SG, as follows:

1) Effect of Unbalancing at Base Load: In the first scenario, the load is at the base case (i.e, $l = 1$ p.u.), and the system is perturbed with a short-duration three-phase fault at $t = 1$ s, so that the critical system modes can be obtained using the identification approach. This is used to study the system stability under various unbalanced conditions at low loading levels, demonstrating the impact of unbalancing on the stable system. Table V illustrates the damping factors and frequency of the critical poles at the base load for different unbalanced conditions. Note that as k increases, the frequency decreases, while the damping factor increases; similar observations were reported in [10] and [40].

2) Effect of Unbalancing on High Loading Levels: In the second scenario, the system load is increased close to its maximum value ($l = 2.2$ p.u.), and the machine is then connected at $t = 0.5$ s. This is used to study the stability of the system for various unbalance conditions at high loading levels, demonstrating how unbalancing leads the system to instability. Figure 14 illustrates the critical poles of the SG speed for various levels of unbalanced conditions. Observe that, beyond $k = 15\%$, the critical pole crosses the imaginary axis and thus the system experiences a Hopf bifurcation with 1.91 Hz

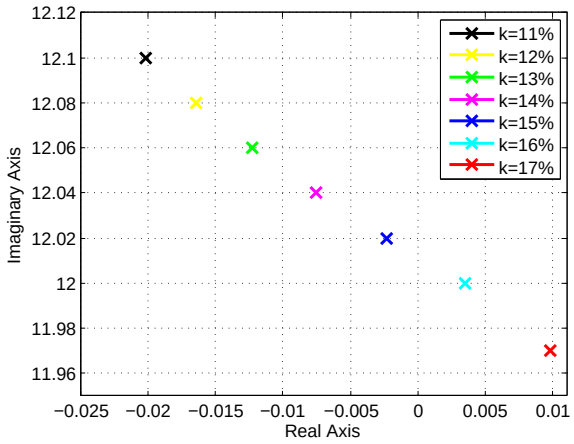

Fig. 14. Zero-pole map of SG speed around critical unbalanced conditions.

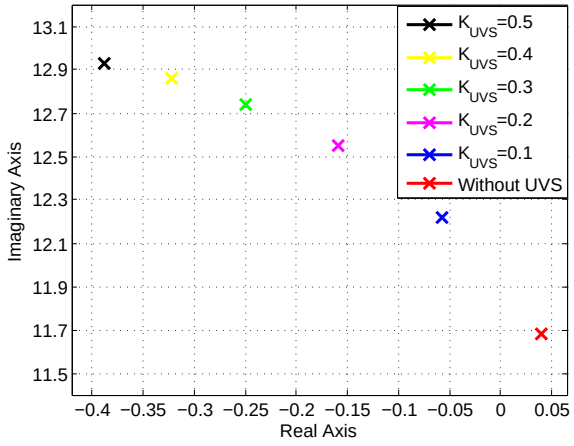

Fig. 15. Critical poles of SG speed associated with the oscillatory mode with and without UVS.

frequency.

For a loading level of 2.2 p.u. and unbalancing of $k = 25\%$, the system is unstable as the critical poles of the SG speed move to the right side of the imaginary axis. This can be corrected by introducing the proposed UVS. Thus, Fig.15 shows the effects of UVS on the critical poles for different K_{UVS} values. Note that as the gain of UVS increases, the critical poles move to the left side of the imaginary axis and the system becomes more stable. Figure 16 illustrates the generator speed with and without UVS at $l = 2.2$ p.u., $k = 25\%$, and $K_{UVS} = 0.2$, when the machine is connected, showing that the generator speed is sufficiently damped and the system becomes stable with the UVS.

E. UVS Impact on DFIG

In order to compare existing control strategies and the proposed UVS for the DFIG, the following scenarios are studied for $k = 15\%$ and $l = 1.15$ p.u.:

- $S1$: This is the classical control balanced approach, which does not take into account the possibility of unbalanced voltages. In this case, the synchronous reference-frame is aligned with the stator flux and has no negative sequence injections.

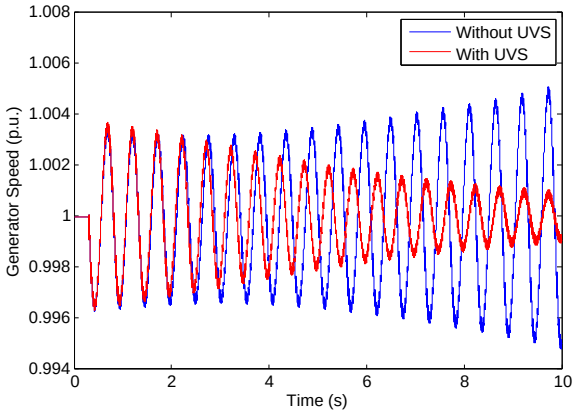

Fig. 16. Transient behavior of SG speed with and without UVS.

- $S2$: This case is based on limiting the electrical torque oscillations in (17); thus, the negative sequence components are adjusted to limit the electrical torque.
- $S3$: This case is based on limiting the stator active power in (18); thus, the negative sequence rotor currents are adjusted to limit the stator active power oscillations.
- $S4$: This is the same as $S1$ with the UVS added.
- $S5$: This is the same as $S2$ with the UVS added.
- $S6$: This is the same as $S3$ with the UVS added.

The output active and reactive powers are set at $P_{out} = 1$ MW, and $Q_{out} = 0$ Mvar, respectively. Based on different control targets, Fig.17 depicts the simulated results with the various control strategies for PF control mode. The control was initially set to $S1$ and changed to $S2$ at $t = 2$ s, and then to $S3$ at $t = 3$ s, respectively. During the simulation, the grid-side converter was enabled, then the DFIG stator was energized, and finally the machine was connected at $t = 0.5$ s; thus, the DFIG is in steady-state after 1 s. Since the transient behaviour of the starting process is not the focus of this paper, this process is not shown in any of the plots. Observe that when the controller is set to $S1$, the negative sequence components of rotor current references are zero; hence, the active and reactive powers, electrical torque, stator voltage and current all contain significant oscillations at 120 Hz, which may damage the DFIG. In the rotor side, the currents contain both the fundamental component of the rotor mechanical frequency minus the stator frequencies $(f_r - f_s)$ and the harmonic component of $(f_s + f_r)$. At $t = 2$ s, the control in $S2$ is activated, resulting in the torque oscillations being reduced over 90% compared to $S1$; however, the power oscillations increase. On the other hand, when the control in $S3$ is activated, the opposite takes place, i.e., the torque oscillations increase but the power oscillations decrease.

Figure 18 illustrates the results of the DFIG with voltage control, but without UVS. In this case, the reference voltage is set at 1.03 p.u. to operate the system within the voltage limits. Observe that the system becomes unstable for $S2$ and $S3$, whereas it was stable under balanced conditions; hence, the voltage unbalance leads to instability.

Figure 19 depicts the results of the DFIG in voltage control mode with UVS. Thus, $S5$ takes place at $t = 2$ s, and $S6$

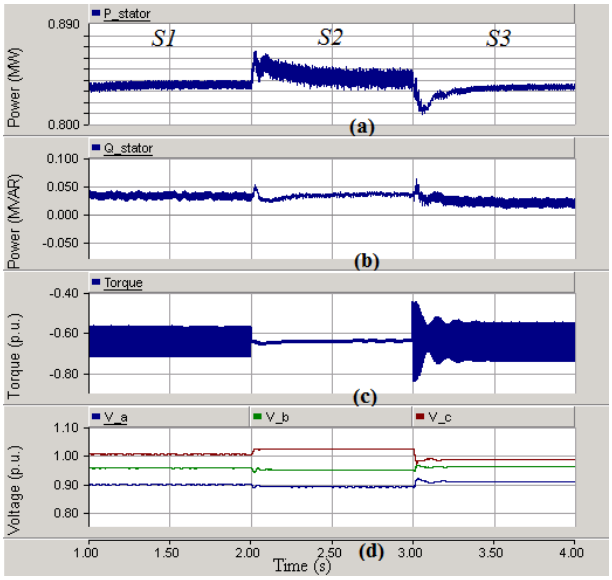

Fig. 17. Transient behaviour of DFIG with various control strategies for PF control mode: (a) stator active power; (b) stator reactive power; (c) electrical torque; (d) voltage magnitude of the load.

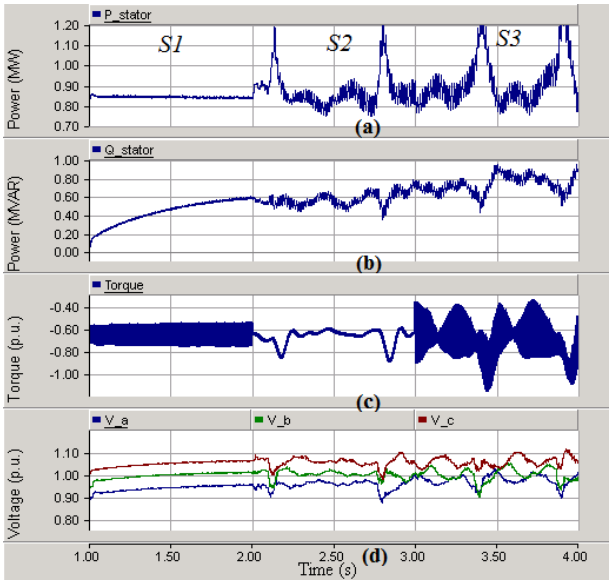

Fig. 18. Transient behaviour of DFIG with various control strategies for voltage control mode without UVS: (a) stator active power; (b) stator reactive power; (c) electrical torque; (d) voltage magnitude of the load.

occurs at $t = 3$ s. Note that the system is now stable and the electrical torque oscillations are reduced, with the best overall system performance being observed for $S5$. This demonstrates the clear advantage of introducing the proposed UVS for unbalanced system operation.

IV. Conclusions

This paper concentrated on the stability analyses of SG and DFIG based DGs in the context of distribution systems under unbalanced conditions. Voltage stability analyses were performed based on PV curves obtained from both power flow and dynamic studies; transient stability studies were carried out

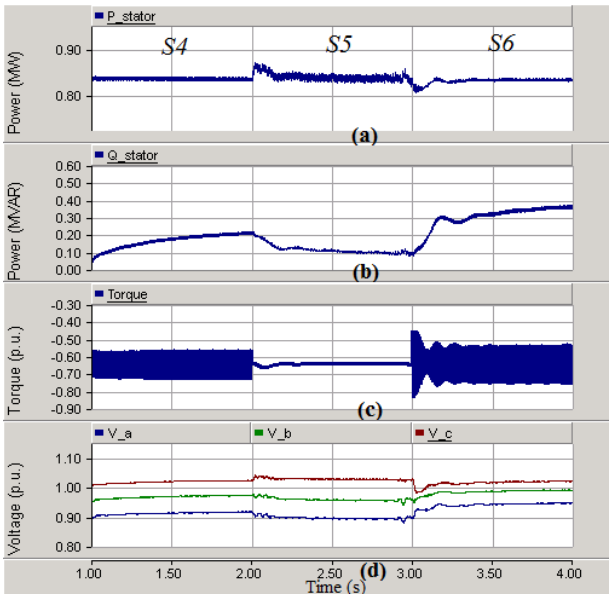

Fig. 19. Transient behaviour of DFIG with various control strategies for voltage control mode with UVS: (a) stator active power; (b) stator reactive power; (c) electrical torque; (d) voltage magnitude of the load.

based on detailed time-domain simulations of contingencies; and small-perturbation stability studies were performed based on identification methods. The PV curves showed that the loadability of the system decreased as unbalancing increases, and from the point of view of transient stability, the time-domain simulations demonstrated that the system was less stable as unbalancing increased; another interesting result was that, as the system load increased, the critical poles crossed the imaginary axes and the system became unstable as unbalancing increased. An unbalanced voltage stabilizer was proposed to improve the stability of the system, demonstrating the effectiveness of the stablizer by eigenvalue analyses and time-domain simulations.

Appendix

Table VI presents the system parameters used in this paper, assuming a simple decoupled impedance line model. The SG data were extracted from [3]. Table VII shows the DFIG parameters. The SG voltage regulator, PI controllers, and UVS parameters are shown in Tables VIII, IX, and X, respectively.

TABLE VI
System Parameters.

S_{base}(MVA)	10
Voltage rating (kV)	2.4
Line impedance (Z_1) (p.u.)	0.035 + j 0.21
Line impedance (Z_2) (p.u.)	0.35 + j 2.1

Acknowledgment

The authors would like to thank Dr. Rodrigo Andrade Ramos from the University of So Paulo, Brazil, for his insightful comments and suggestions.

TABLE VII
DFIG PARAMETERS.

Power rating (MVA)	1.717
Voltage rating (kV)	0.69
Stator/rotor turn ratio	0.335
R_s (p.u.)	0.005049
R_r (p.u.)	0.00357
L_s (p.u.)	0.1226
L_r (p.u.)	0.1118
L_m (p.u.)	2.0773
$2H$ (sec)	4.55

TABLE VIII
SG VOLTAGE REGULATOR PARAMETERS.

Maximum regulator voltage (p.u.)	6
Minimum regulator voltage (p.u.)	0
Regulator gain	78
Regulator pole (sec)	10
Regulator zero (sec)	1
Time constant of the field circuit T_d (sec)	1

TABLE IX
PI CONTROLLERS PARAMETERS.

	PI_1	PI_2	PI_3	PI_4	PI_5
Proportional gain	1	0.5	5	10	10
Integral time constant (sec)	0.1	0.2	0.05	0.01	0.01

TABLE X
UVS PARAMETERS.

	SG	DFIG
K_{UVS}	0.2	1.1
T_{U1} (sec)	0.125	0.125
T_{U2} (sec)	0.030	0.030
V_{UVS}^{max} (p.u.)	0.2	0.2
V_{UVS}^{min} (p.u.)	-0.2	-0.2

REFERENCES

[1] M. Reza, J. G.Slootweg, P. H. Schavemaker, W. L. Kling, and L. V. der Sluis, "Investigating impacts of distributed generation on transmission system stability," in *Proc. IEEE Power Tech Conference*, Bologna, Jun. 2003.

[2] A. M. Azmy and I. Erlich, "Impact of distributed generation on the stability of electrical power system," in *Proc. IEEE PES General Meeting*, Jun. 2005.

[3] E. Nasr-Azadani, C. Canizares, and K. Bhattacharya, "Modeling and stability analysis of distributed generation," in *Proc. IEEE PES General Meeting*, Jul. 2012.

[4] S. Granville, P. Lino, F. Ralston, L. A. Barroso, and M. Pereira, "Recent advances of sugarcane biomass cogeneration in brazil," in *Proc. IEEE PES General Meeting*, Jul. 2009.

[5] M. Wang and J. Zhong, "Development of distributed generation in china," in *Proc. IEEE PES General Meeting*, Jul. 2009.

[6] M. Arriaga, C. A. Caizares, and M. Kazerani, "Renewable energy alternatives for remote communities in northern ontario, canada," *IEEE Trans. Sustainable Energy*, vol. 4, no. 3, pp. 661–670, 2013.

[7] T. Ackermann, *Wind Power in Power Systems*. NJ: Wiley: Hoboken, 2005.

[8] X.-P. Zhang, P. Ju, and E. Handschin, "Voltage stability analysis in unbalanced power systems by optimal power flow," *IEEE Trans. Power Syst.*, vol. 20, no. 3, pp. 1320–1329, Aug. 2005.

[9] D. Lauria and P. Varilone, "Continuation three-phase power flow: A tool for voltage stability analysis of unbalanced three-phase power systems," *Proc. IET Gen., Trans. and Dist.*, vol. 153, no. 3, pp. 261–268, May 2006.

[10] R. H. Salim and R. A. Ramos, "A model-based approach for small-signal stability assessment of unbalanced power systems," *IEEE Trans. Power Syst.*, vol. 27, no. 4, pp. 1184–1190, Nov. 2012.

[11] ——, "A framework for analyzing the small-signal dynamic performance of unbalanced power systems," in *Proc. IEEE PES General Meeting*, Jul. 2011.

[12] R. G. Harley, E. B. Makram, and E. G. Duran, "The effects of unbalanced networks and unbalanced faults on induction motor transient stability," *IEEE Trans. Energy Convers.*, vol. 3, no. 2, pp. 398–403, 1988.

[13] E. B. Makram, V. O. Zambrano, R. G. Harley, and J. C. Balda, "Three-phase modeling for transient stability of large scale unbalanced distribution systems," *IEEE Trans. Power Syst.*, vol. 4, no. 2, pp. 487–493, 1989.

[14] R. G. Harley, E. B. Makram, and E. G. Duran, "The effects of unbalanced networks on synchronous and asynchronous machine transient stability," *Elect. Power Syst. Res.*, vol. 13, no. 2, pp. 119–127, 1987.

[15] E. B. Makram, V. O. Zambrano, and R. G. Harley, "Synchronous generator stability due to multiple faults on unbalanced power systems," *Elect. Power Syst. Res.*, vol. 15, no. 1, pp. 31–39, 1988.

[16] V. Akhmatov, "Analysis of dynamic behaviour of electric power systems with large amount of wind power," Ph.D. dissertation, Technical university of Denmark, Lyngby, Denmark, 2003.

[17] A. P. Grilo, A. d. A. Mota, L. T. M. Mota, and W. Freitas, "An analytical method for analysis of large-disturbance stability of induction generators," *IEEE Trans. Power Syst.*, vol. 22, no. 4, pp. 1861–1869, 2007.

[18] M. Reza, "Stability analysis of transmission systems with high penetration of distributed generation," Ph.D. dissertation, Delft University of Technology, Delft, Netherlands, 2006.

[19] I. Xyngi, A. Ishchenko, M. Popov, and L. van der Sluis, "Transient stability analysis of a distribution network with distributed generators," *IEEE Trans. Power Syst.*, vol. 24, no. 2, pp. 1102–1104, May 2009.

[20] P. Ledesma and J. Usaola, "DFIG model for transient stability analysis," *IEEE Trans. Energy Convers.*, vol. 20, no. 2, pp. 388–397, Jun. 2005.

[21] Y. Lei, A. Mullane, G. Lightbody, and R. Yacamini, "Modeling of the wind turbine with a DFIG for grid integration studies," *IEEE Trans. Energy Convers.*, vol. 21, no. 1, pp. 257–264, Mar. 2006.

[22] D. Xiang, L. Ran, P. Tavner, and S. Yang, "Control of a DFIG in a wind turbine during grid fault ride through," *IEEE Trans. Energy Convers.*, vol. 21, no. 3, pp. 652–662, Sep. 2006.

[23] J. Morren and S. de Haan, "Ride through of wind turbines with DFIG during a voltage dip," *IEEE Trans. Energy Convers.*, vol. 20, no. 2, pp. 435–441, Jun. 2008.

[24] ——, "Short-circuit current of wind turbines with DFIG," *IEEE Trans. Energy Convers.*, vol. 22, no. 1, pp. 174–180, Mar. 2007.

[25] O. Gomis-Bellmunt, A. Junyent-Ferre, A. Sumper, and J. Bergas-Jan, "Ride-through control of a DFIG under unbalanced voltage sags," *IEEE Trans. Energy Convers.*, vol. 23, no. 4, pp. 1036–1045, Dec. 2008.

[26] L. Xu and Y. Wang, "Dynamic modeling and control of DFIG-based wind turbines under unbalanced network conditions," *IEEE Trans. Power Syst.*, vol. 22, no. 1, pp. 1320–1329, Feb. 2007.

[27] Y. Zhou, P. Bauer, J. Ferreira, and J. Pierik, "Operation of grid-connected DFIG under unbalanced grid voltage condition," *IEEE Trans. Energy Convers.*, vol. 24, no. 1, pp. 240–246, Mar. 2009.

[28] T. K. A. Brekken and N. Mohan, "Control of a doubly fed induction wind generator under unbalanced grid voltage conditions," *IEEE Trans. Energy Convers.*, vol. 22, no. 1, pp. 129–135, Mar. 2007.

[29] R. Pena, R. Cardenas, E. Escobar, J. Clare, and P. Wheeler, "Control system for unbalanced operation of stand-alone DFIGs," *IEEE Trans. Energy Convers.*, vol. 22, no. 2, p. 544545, Jun. 2007.

[30] L. Yang, Z. Xu, J. Ostergaard, Z. Y. Dong, K. Wong, and X. Ma, "Oscillatory stability and eigenvalue sensitivity analysis of a DFIG wind turbine system," *IEEE Trans. Energy Convers.*, vol. 26, no. 1, pp. 328–339, Mar. 2011.

[31] *PSCAD/EMTDC ver 4.2 Users Manual*, Manitoba HVDC Research Centre Inc., Winnipeg, Manitoba, Canada.

[32] P. Kundur, *Power System Stability and Control*. New York: McGraw-Hill, 1994.

[33] R. H. Salim and R. A. Ramos, "Analyzing the effect of the type of terminal voltage feedback on the small signal dynamic performance of synchronous generators," in *Proc. IREP Symp. Bulk Power System Dynamics and Control*, Aug. 2010.

[34] N. Mohan, T. M. Undeland, and W. Robbins, *Power electronics: converters, applications, and design*. New York: Wiley, 2007.
[35] "Voltage stability assessment: Concepts, practices and tools," IEEE/PES Power System Stability Subcommittee, Tech. Rep., Aug. 2002.
[36] W. H. Kersting, *Distribution System Modeling and Analysis*. CRC Press, 2006.
[37] M. Z. Kamh and R. Iravani, "Unbalanced model and power-flow analysis of microgrids and active distribution systems," *IEEE Trans. Power Del.*, vol. 25, no. 4, pp. 2851–2858, Oct. 2010.
[38] *MATLAB*, The MathWorks Inc.
[39] A. G. Exposito, A. J. Conejo, and C. Canizares, *Electric Energy Systems, Analysis and Operation*. CRC Press, 2009.
[40] R. H. Salim, R. A. Ramos, and N. G. Bretas, "Analysis of the small signal dynamic performance of synchronous generators under unbalanced operating conditions," in *Proc. IEEE PES General Meeting*, Jul. 2010.
[41] H. Ghasemi, "On-line monitoring and oscillatory stability margin prediction in power systems based on system identification," Ph.D. dissertation, University of Waterloo, Waterloo, Canada, 2006.
[42] K. Steiglitz and L. E. McBride, "A technique for the identification of linear systems," *IEEE Trans. Autom. Control*, vol. AC-10, pp. 461–464, 1965.
[43] S. Li, K. Tomsovic, and T. Hiyama, "Load following functions using distributed energy resources," in *Proc. IEEE PES Summer Meeting Meeting*, Jul. 2000.

Ehsan Nasr-Azadani (S'11) received his M.Sc. degree in Electrical Engineering from the Amirkabir University, Tehran, Iran, in 2009, and is currently pursuing the Ph.D. degree in Electrical Engineering at the University of Waterloo, Waterloo, ON, Canada. His research interests are in modeling, control, and stability issues in microgrids.

Claudio A. Cañizares (S'86, M'91, SM'00, F'07) received the electrical engineer diploma from the Escuela Politécnica Nacional (EPN), Quito, Ecuador, in 1984 and the M.S. and Ph.D. degrees electrical engineering are from the University of Wisconsin-Madison in 1988 and 1991, respectively. He has held various academic and administrative positions at the Electrical and Computer Engineering Department of the University of Waterloo, Waterloo, ON, Canada, since 1993, where he is currently a full Professor, the Hydro One Endowed Chair, and an Associate Director of the Waterloo Institute for Sustainable Energy (WISE). His research activities concentrate in the study of stability, optimization, modeling, simulation, control, and computational issues in power systems within the context of competitive electricity markets and smart grids.

Dr. Cañizares has been the recipient of various IEEE-PES Working Group awards and holds and has held several leadership appointments in IEEE-PES technical committees and subcommittees. He is a registered Professional Engineer in the province of Ontario and a Fellow of the Royal Society of Canada and of the Canadian Academy of Engineering.

Daniel E. Olivares (S'11) was born in Santiago, Chile, and received the B.Sc. and the Engineer degree in electrical engineering from the University of Chile in Santiago in 2006 and 2008, respectively. He finished his Ph.D. studies in Electrical and Computer Engineering at the University of Waterloo, Waterloo, ON, Canada, in January 2014. His research interests include modeling, simulation, control and optimization of power systems in the context of smart grids.

Kankar Bhattacharya (M'95, SM'01) received the Ph.D. degree in electrical engineering from the Indian Institute of Technology, New Delhi, India, in 1993. He was in the faculty of Indira Gandhi Institute of Development Research, Mumbai, India, during 1993-1998, and then the Department of Electric Power Engineering, Chalmers University of Technology, Gothenburg, Sweden, during 1998-2002. He joined the E&CE Department of the University of Waterloo, Waterloo, ON, Canada, in 2003 where he is currently a full Professor. His research interests are in power system economics and operational aspects